Nano Research

ISSN 1998-0124 CN 11-5974/O4
https://doi.org/10.1007/s12274-023-6363-x

Research Article

In vivo real-time monitoring delayed administration of M2 macrophages to enhance healing of tendon by NIR-II fluorescence imaging

Yuzhou Chen[1,2,§], Mo Chen[1,3,§], Chengxuan Yu[1,§], Huizhu Li[1], Liman Sai[4], Nguyen T. K. Thanh[5,6], Yueming Wang[7], Yan Wo[7], Jian Zhang[1], Xing Yang[8], Evgenii L. Guryev[9], Andrei V. Zvyagin[9], Hao De[10], Min Tang[11], Shiyi Chen[1], Yunxia Li[1] (✉), Yuefeng Hao[8] (✉), Sijia Feng[1] (✉), and Jun Chen[1] (✉)

[1] *Sports Medicine Institute of Fudan University, Department of Sports Medicine, Huashan Hospital, Fudan University, Shanghai 200040, China*
[2] *Department of Orthopedic Surgery, Xinhua Hospital Affiliated to Shanghai Jiao Tong University School of Medicine, Shanghai 200092, China*
[3] *Department of Bone and Joint Surgery, Department of Orthopedics, Renji Hospital, School of Medicine, Shanghai Jiao Tong University, Shanghai 200001, China*
[4] *Department of Physics, Shanghai Normal University, Shanghai 200234, China*
[5] *Biophysics Group, Department of Physics and Astronomy, University College London, London WC1E 6BT, UK*
[6] *UCL Healthcare Biomagnetic and Nanomaterials Laboratories, London W1S 4BS, UK*
[7] *Department of Anatomy and Physiology, School of Medicine, Shanghai Jiao Tong University, Shanghai 200025, China*
[8] *Department of Orthopedics, Affiliated Suzhou Hospital of Nanjing Medical University, Suzhou 215500, China*
[9] *Institute of Biology and Biomedicine, Lobachevsky State University of Nizhny Novgorod, Nizhny Novgorod 603950, Russia*
[10] *Mathematical Institute, University of Oxford, Oxford OX2 6GG, UK*
[11] *Institute of Natural Sciences, School of Mathematics, Shanghai Jiao Tong University, Shanghai 200240, China*
[§] *Yuzhou Chen, Mo Chen, and Chengxuan Yu contributed equally to this work.*

Received: 12 September 2023 / **Revised:** 23 November 2023 / **Accepted:** 23 November 2023

ABSTRACT

The administration time is a critical but long-neglected point in cell therapy based on macrophages because the incorrect time of macrophage administration could result in diverse outcomes regarding the same macrophage therapy. In this work, the second near-infrared (NIR-II) fluorescence imaging *in vivo* tracking of M2 macrophages during a pro-healing therapy in the mice model of rotator cuff injury revealed that the behavior of administrated macrophages was influenced by the timing of their administration. The delayed cell therapy (DCT) group had a longer retention time of injected M2 macrophages in the repairing tissue than that in the immediate cell therapy (ICT) group. Both Keller–Segel model and histological analysis further demonstrated that DCT altered the chemotaxis of M2 macrophages and improved the healing outcome of the repaired structure in comparison with ICT. Our results offer a possible explanation of previous conflicting results on reparative cell therapy and provoke reconsideration of the timing of these therapies.

KEYWORDS

macrophage, cell therapy, NIR-II, *in vivo* imaging, delayed therapy, tendon healing

1 Introduction

M2 macrophages aid in healing and regeneration of injured tissues, inspiring the cell therapy that introduces M2 macrophages for immunomodulation and improvement of healing outcome. Nonetheless, M2 macrophage therapy, like many other therapies employing reparative cells (typically stem cells), sometimes failed to achieve expected therapeutic functions [1–3]. The timing of M2 macrophage enhancement as a postulation among previous studies has drawn attention of investigators, as there is always an interval, specifically several days, between the onset of injury and detection of M2 macrophages within tissues [4]. Moreover, interference of early inflammation in injured tissues might result in an interrupted switch to the phase of healing [5, 6]. Besides, administration of reparative cells evading acute inflammation may provide benefits for accumulation, survival, and functioning of these cells owing to suitable micro-environment [7].

Research on the delayed M2 macrophage therapy has emerged in recent years, in which the cells were not introduced immediately after the injury like the classical immediate therapy. With a scan of the current literature, it was noticed that diverse responses to immediate therapies with M2 macrophages were demonstrated [1, 2, 8–10], while delayed therapies by promotion of M2 polarization presented improvements under variable conditions, including inflammatory bowel disease, hindlimb ischemia, and spinal cord injury [11–15]. However, efforts were paid in these studies to evaluate if M2 macrophages achieved

Address correspondence to Yunxia Li, liyunxia912@aliyun.com; Yuefeng Hao, 13913109339@163.com; Jun Chen, biochenjun@fudan.edu.cn; Sijia Feng, 815954681@qq.com

therapeutic effects, and information about distribution and movements of introduced cells was unavailable. Hence, the underlying mechanism of such a difference was unable to be interpreted owing to a lack of knowledge regarding the monitoring of cells after *in vivo* administration.

Nowadays, fluorescence imaging is widely utilized in medical science, and the second near-infrared window (NIR-II, 1000–1700 nm) is recognized as one of the most promising fluorescence *in vivo* imaging technique with minimal scattering, high signal-to-noise quotient (SNQ), and low self-fluorescence background compared with visible light and the first near-infrared window (NIR-I, 700–900 nm) [16–19]. In previous studies, labelling and tracking of mesenchymal stem cells in mice by lead sulfide quantum dots (PbS QDs) with emission in NIR-II window successfully revealed the fate of injected cells [20]. Consequently, *in vivo* monitoring of M2 macrophages with NIR-II imaging based on PbS QDs may hopefully unveil a possible explanation of the restricted effect of immediate M2 macrophage therapy and advantages of delayed therapy by presenting differences in cell migration and retention in a non-invasive and real-time manner, from which a potential direction to improve not only M2 macrophage therapy but other therapies employing reparative cells may be derived.

The current study began with synthesis of PbS QDs, which were then conjugated to Tat peptide and used to label M2 macrophages (Fig. 1(a)). After that, sensitivity and stability of PbS QDs labeled M2 macrophages for *in vivo* imaging were studied. Next, mice models of acute injury and surgical repair of the supraspinatus tendon were prepared, a situation that had been proven to require efficient pro-healing therapies. The PbS QDs labeled M2 macrophages were injected to the shoulder joints of animal models immediately or on the 7th day post-operation (Fig. 3(a)) and were tracked with the NIR-II fluorescence imaging in a time course. Simultaneously, changes of immune system and treated tendons after cell therapy were followed correspondingly through analysis of peripheral leukocyte subsets and micro-magnetic resonance imaging (mMRI). Finally, the efficacy of immediate and delayed M2 macrophage therapy was assessed and compared by pathological analysis. With longitudinal monitoring of M2 macrophages injected at different timepoints, this work aims at describing patterns of cell behavior to provoke reconsiderations of the timing of M2 macrophage therapy.

2 Materials and methods

2.1 Reagents and materials

All reagents were bought as products and used without further modification. Working solutions were prepared with deionized water generated by an ELGA Purelab classic UVF system. Bovine pancreatic ribonuclease-A (RNase-A, M_w: 13.7 kDa, > 70 U/mg), lead acetate trihydrate ($Pb(OAc)_2{\cdot}3H_2O$, ≥ 99.9%), sodium sulfide nonahydrate ($Na_2S{\cdot}9H_2O$, ≥ 98.0%), sodium hydroxide (NaOH, ≥ 98.0%), and N-hydroxysuccinimide (NHS) were purchased from Sigma-Aldrich. 1-Ethyl-3-(3-dimethylaminopropyl) carbon diimine hydrochloride (EDC) was purchased from Thermo Fisher Scientific. Sterile 1× phosphate buffer solutions (PBS) with a pH of 7.4 were adopted when mentioned.

2.2 Animals

Male C57BL/6 mice (8-week old, 24–28 g) and Balb/c nude mice (8-week old, 20–22 g) were bought from Shanghai Jie Si Jie Laboratory Animal Co. Ltd (Shanghai, China). All animal experiments were in strict accordance with the guidelines of the Chinese Council for Animal Care.

2.3 Instrumentation

Microwave reactor (Discover, CEM) with a cooling system was utilized for microwave synthesis of PbS QDs. The freshly synthesized PbS QDs were purified by ultra-centrifugation in ultra-centrifugal filter tubes (Amicon, molecular weight cutoff (MWCO): 10 kDa). An NS1 NanoSpectralyzer fluorimetric analyzer with λ_{ex} = 808 nm was used for NIR-II fluorescence spectra measurement. The NIR-II fluorescence images were obtained from an *in vivo* imaging system (MARS, Artemis Intelligent Imaging, Shanghai, China). The excitation shadowless illumination was provided by a fiber-coupled 808 nm laser. A 1250 nm long-pass filter was adopted to filter the emission light before it reached the camera. Emitted light was collimated by a 50 mm focal length SWIR lens (MARS-FAST, Artemis Intelligent Imaging, Shanghai, China). The fluorescence was then detected by a liquid-nitrogen-cooled InGaAs camera (NIRvana 640, Teledyne Princeton Instruments) located right above the working stage, irradiating the subject vertically.

2.4 Synthesis of PbS QDs

Firstly, 500 μL of RNase-A (50 mg/mL) solution and 500 μL of $Pb(OAc)_2$ (10 mM) solution were mixed to prepare the RNase-A/Pb^{2+} solution. Then, 50 μL of NaOH solution (1 M) was added to the precursor solution to basify the pH to 9–11 with stirring for 5 min. After that, 50 μL of freshly prepared Na_2S (10 mM) solution was added to the mixed solution. Quickly after putting into a stir bar, the tube with mixture was inserted into a microwave reactor with a heating temperature at 70 °C for 30 s under an input power of 30 W. At the formation of PbS QDs, the mixture turned into transparent dark brown. The freshly prepared PbS QDs were then ultra-filtered for purification. Then the solution was rinsed by PBS to remove excessive reagents. The as-prepared PbS QDs were stored at 4 °C in darkness.

2.5 Macrophage collection

According to previous study [21], bone marrow mononuclear cells (BMMCs) were isolated from the femur and tibia bones of C57BL/6 mice and briefly treated with red blood cell-lysing ammonium chloride potassium (ACK; 150 mM ammonium chloride, 10 mM potassium bicarbonate, and 10 μM ethylenediaminetetraacetic acid (EDTA)) prior to being cultured (37 °C at 5% CO_2 concentration) in Roswell Park Memorial Institute (RPMI)-1640 complete medium (10% fetal bovine serum (FBS), 1 mM glutamate, 1 mM sodium pyruvate, 100 units/mL penicillin, and 100 μg/mL streptomycin (all purchased from BioService, Wuhan, China)). The culture medium was entirely discarded on day 3 and 6 and replaced by fresh warmed medium with granulocyte-macrophage colony-stimulating factor (GM-CSF) (20 ng/mL). On day 6, non-adherent cells in the culture supernatant were discarded by gentle washing with PBS, and the remaining adherent cells were considered M0 macrophages. For *in vitro* M2 polarization, 10 ng/mL of IL-4 (Peprotech) were added to RPMI-1640 complete medium on day 6 for 24–48 h. After polarization, non-adherent cells in the culture supernatant were discarded.

2.6 Cell labeling

As described in our previous work [21], the pH of PbS QDs solution was adjusted to 5.5–6.5 by NaOH and HCl. 2 EDC and NHS were added into PbS QDs solution and the mixture was vibrated at room temperature for30 min. Next, PbS QDs were covalently bonded with Tat peptide using crosslinking reagent Sulfo-SMCC (Lei et al., 2008). After overnight reaction at 4 °C, the mixture was centrifuged using ultrafiltration tube to remove the

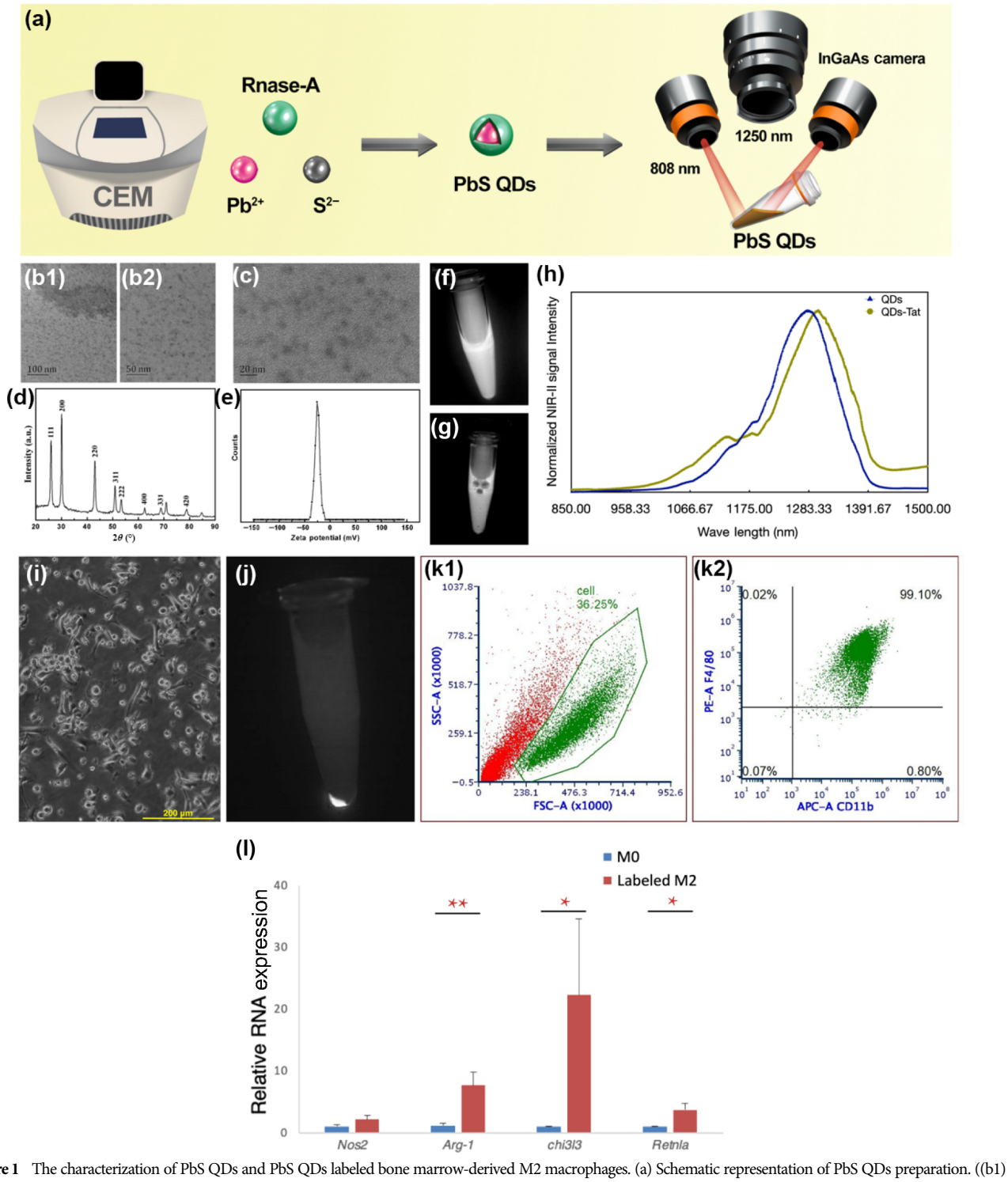

Figure 1 The characterization of PbS QDs and PbS QDs labeled bone marrow-derived M2 macrophages. (a) Schematic representation of PbS QDs preparation. ((b1) and (b2)) TEM images, (c) HRTEM images, (d) X-ray diffraction (XRD) pattern, and (e) zeta-potential measurement of the PbS QDs. (f) NIR-II imaging (λ_{ex}: 808 nm, exposure time: 10 ms) of PbS QDs in an Eppendorf tube. (g) NIR-II imaging (λ_{ex}: 808 nm, exposure time: 10 ms) of Tat-PbS QDs in an Eppendorf tube. (h) Normalized fluorescence spectra of PbS QDs and Tat-PbS QDs. (i) Micrographs of bone marrow-derived M2 macrophages. (j) NIR-II imaging (λ_{ex}: 808 nm, exposure time: 10 ms) of PbS QDs labeled M2 macrophages in an Eppendorf tube after centrifugation. ((k1) and (k2)) Representative flow cytometry analysis of PbS QDs labeled M2 macrophages. (l) The analysis of the markers of M2 macrophages quantitative RT-PCR.

unbound free impurities. Then, the M2 macrophages were co-incubated with Tat-PbS QDs for about 3 h. After that, PBS (pH = 7.4) was used to wash away the Tat-PbS QDs that failed to label macrophages.

2.7 Flow cytometry of labeled M2 macrophages

PbS QDs labeled M2 macrophages were suspended in 100 μL PBS. Then the sample was centrifuged at 1200 rpm for 5 min and rinsed by 1 mL of PBS. After fluorescent staining with antibodies (PE anti-mouse F4/80, APC anti-mouse CD11b, Biolegend) for 30 min at 4 °C, the sample was rinsed by 1 mL of PBS again and resuspended with 300 μL of PBS. Percentage of $F4/80^{+}CD11b^{+}$ cells was calculated and analyzed by flow cytometry.

2.8 Reverse transcription polymerase chain reaction (RT-PCR) of labeled M2 macrophages

RNA was obtained using the TRIZOL method (Invitrogen), and complementary DNA (cDNA) was synthesized from 1 μg of total

RNA using iSCRIPT reverse transcriptase. RT-PCR for arginase-1 (*Arg-1*), *iNOS*, *Chi3l3*, and *Retnla* was performed using primer sequences and conditions reported previously. Products were electrophoresed through 2% agarose gels containing 0.5 μg/mL ethidium bromide. RNA expression was normalized to glyceraldehyde 3-phosphate dehydrogenase (GAPDH) expression by the $2^{-\Delta Ct}$ method.

2.9 *In vivo* assessment of sensitivity and stability of labeled M2 macrophages

The PbS QDs labeled M2 macrophages (5×10^2, 1×10^3, 5×10^3, 2×10^4, 5×10^4, and 2×10^5 cells) in PBS (20 μL) were injected subcutaneously into the dorsum of BALB/c nude mice. NIR-II fluorescence images of the mice were collected on days 0, 7, 14, 21, 28, and 35 after injection. All the images were collected using an NIR *in vivo* imaging system as described above, with an exposure time of 250 ms. The calibrated NIR-II fluorescent intensity of labeled M2 macrophages was analyzed by ImageJ software.

2.10 Preparation of experimental animal models

C57BL/6 mice were employed in animal experiments. The animal models were prepared as previously described [21] and as shown in Fig. S1 in the Electronic Supplementary Material (ESM). After repairing the supraspinatus tendon, for the mice treated by M2 macrophage therapy [20, 22], 2×10^5 labeled M2 macrophages were administered immediately (immediate cell therapy (ICT)) or on the 7th day (delayed cell therapy (DCT)). For the mice served as the control group of NIR-II imaging, the mice were intra-articularly injected with 40 μL of PbS QDs immediately (immediate therapy-QDs (IT QDs)) or after 7 days (delayed therapy-QDs (DT QDs)). As for the control group in peripheral blood tests, mMRI examinations, and histological analysis, 40 μL of PBS was injected. Then the mice were raised in cages under the same circumstances. The mice were kept alive until 63 days (9 weeks) after repair surgery.

2.11 *In vivo* observation

NIR-II fluorescence images and radiography images were collected on days 1, 3, 7, 10, 14, 21, 28, and 35 after injection. All the NIR-II fluorescence images were collected using an NIR *in vivo* imaging system as described above, with an exposure time of 250 ms. For radiography, an optical and X-ray small animal imaging system (*In Vivo* Xtreme, Bruker) was used. The NIR-II fluorescent intensity of PbS QDs labeled M2 macrophages in the region of the shoulder and the supraspinatus tendon was analyzed using ImageJ software.

2.12 Analysis of chemotaxis

The following equation was generated based on the Keller–Segel model (KS model) [23] describing chemotaxis of cells and context of the current study. For a point x, which was located on a line from the joint cavity to the lateral edge of the humeral head

$$\frac{\partial \rho}{\partial t}(x,t) = \frac{\partial}{\partial x}\left[D\frac{\partial \rho}{\partial x}(x,t) - \frac{\partial \phi}{\partial x}\rho(x,t)\right] \quad (1)$$

where D represents the diffusion coefficient, $\rho(x)$ represents the value of NIR-II fluorescent intensity (positively related to the number of cells) of a point x, and $\phi(x)$ is the corresponding chemical potential (chemical attractant concentration). At steady state, D is supposed to be a constant, then

$$D\frac{\partial \rho}{\partial x} = \frac{\partial \phi}{\partial x}\rho \quad (2)$$

thereby

$$\frac{1}{\rho}\cdot\frac{\partial \rho}{\partial x} = \frac{1}{D}\cdot\frac{\partial \phi}{\partial x} \quad (3)$$

and

$$\int_0^x \frac{1}{\rho}\cdot\frac{\partial \rho}{\partial x}\mathrm{d}\tilde{x} = \int_0^x \frac{1}{D}\cdot\frac{\partial \phi}{\partial x}\mathrm{d}\tilde{x} \quad (4)$$

hence

$$\log\rho(x) - \log\rho(0) = \frac{1}{D}\cdot\phi(x) - \frac{1}{D}\cdot\phi(0) \quad (5)$$

set $\phi(0) = 0$, then

$$\log\frac{\rho(x)}{\rho(0)} = \frac{1}{D}\cdot\phi(x) \quad (6)$$

consequently

$$\phi(x) \sim \log\frac{\rho(x)}{\rho(0)} \quad (7)$$

On the image acquired at each time point, the NIR-II fluorescent intensity of every pixel forming the line from the joint cavity to the lateral edge of the humeral head ($\rho(x)$) was analyzed using ImageJ software. According to the a forementioned equation, the chemical potential ($\phi(x)$) was then calculated, and a distribution curve was obtained. The positive slope of distribution curve reflected the size of chemotaxis effect of M2 macrophages, which was further calculated and compared between the two groups.

2.13 Peripheral blood test

150 μL of freshly collected peripheral blood from the angular vein of mouse ($N = 3$ at each time point) was collected in a time course (for the DCT group and corresponding control group: the 7th day after operation, 1, 5, 10, 15, 20, 25, and 30 days after cell therapy; for the ICT group and corresponding control group: before surgery, 1, 5, 10, 15, 20, 25, and 30 days after cell therapy). The blood sample was tested by an automatic hematology analyzer (BC-2800vet, Mindray, China) for the total count and classified subsets (neutrophil, lymphocyte, and monocyte) of leukocytes.

2.14 Micro-MRI scan

Micro-MRI scans were performed in a time course (2, 5, and 9 weeks after repair surgery) with a 7.0-T magnetic resonance imaging scanner (Bruker, Belgium) for the ICT and DCT group. The oblique coronal T2 weighted sequence was applied with parameters as follows: relaxation time (TR): 1800 ms, echo time (TE): 35 ms, field of view (FOV): 20 mm × 20 mm, slice thickness: 0.3 mm, flip angle: 90, and total time: 8 min 44 s. All these images were analyzed with ImageJ to evaluate the SNQ of the operated supraspinatus tendon.

2.15 Histopathological analysis

The whole supraspinatus tendon and the humeral head of the left shoulder of the mice were collected (9 weeks post-operation) and stored in 4% paraformaldehyde for at least 24 h to prepare histopathological slides for histopathological analysis. Hematoxylin and eosin (H&E), Masson, Sirius red, and safranin O staining were done according to the methods previous reported [24–26]. Histological images were acquired on an optical microscope (Nikon Eclipse CI, Japan). The scanning images of the histological sections were collected by using the tissue section digital scanner and imaging system. Three randomly chosen areas near the tendon–bone interface of each section were examined, and the averaged histological examination score of the three areas was calculated as the score of this section. For the

immunohistochemical analysis, three different areas of each section were likewise evaluated. The number of CD206 positive cells and nucleated cells was counted, and the averaged proportion of CD206 positive cells was recorded as the proportion of this section.

2.16 Statistical analysis

All data were presented as means and standard deviation (SD) unless otherwise indicated. The comparisons were performed and analyzed using Stata 14.0 software. Continuous variables with normal distributions were analyzed with the student *t* test; otherwise, they were analyzed with the Wilcoxon rank sum test. A P value < 0.05 was considered statistically significant with *, < 0.01 with **, and < 0.001 with ***.

3 Results and discussion

To begin with, PbS QDs with NIR-II fluorescence were synthesized according to our previously published methods (Fig. 1(a)) [27]. Typical transmission electron microscopy (TEM) images are shown in Figs. 1(b1) and 1(b2). The PbS QDs showed sphere structure with good monodispersity with sizes of approximately 5 nm under high resolution TEM (HRTEM) detection (Fig. 1(c)). As shown in Fig. 1(d), the diffraction peaks can be assigned to crystal planes of face-center-cubic rock salt structured PbS (JCPDS No. 005-0592). The sharp peaks indicated well crystallization of the PbS QDs. No impurities were found, revealing their high purity. Figure 1(e) demonstrated that the PbS QDs had a surface potential of −25.7 mV, which could result from negatively charged chemical groups in RNase-A ligand such as carboxyl or hydroxyl. To label M2 macrophages, PbS QDs were conjugated to Tat peptide through the same process that has been previously reported [28]. The water solution of PbS QDs and Tat-PbS QDs demonstrated a strong NIR-II signal when observing by an InGaAs camera within the NIR-II imaging system (Figs. 1(f) and 1(g)). An emission peak of PbS QDs (around 1280 nm) was located in the NIR-II window, as detected by fluorescence spectra (Fig. 1(h)). The emission peak of the Tat-PbS QDs was also located in the NIR-II window with a slight redshift (Fig. 1(h)), which could be attributed to aggregation of PbS QDs after combining with a peptide.

Bone marrow derived macrophages were prepared using the femur and the tibia of mice and were differentiated into M2 macrophages by IL-4 and IL-13, according to previous reports [29] (Fig. 1(i)). M2 macrophages were labeled by PbS QDs-Tat according to the procedure detailed previously [28], harvested, and washed by PBS, after which the pellet of labeled M2 macrophages showed a strong NIR-II signal while the supernatant showed no NIR-II signal (Fig. 1(j)).

After labelling, M2 macrophages were examined according to previous reports to determine if the polarization status was maintained [13]. Labeled M2 macrophages were first characterized by flow cytometry. As shown in Figs. 1(k1) and 1(k2), a high proportion of CD11b+F4/80+ macrophages was observed among the labeled cells. Furthermore, when compared with M0 macrophages, quantitative RT-PCR revealed fundamentally increased expression of genes indicative of M2 polarization (*Arg-1*, *Chi3l3*, and *Retnla*) of labeled M2 macrophages (Fig. 1(l)).

The sensitivity and stability of M2 macrophages labeled by PbS QDs for NIR-II imaging *in vivo* were validated before cell therapy. As shown in Fig. 2(a), different concentrations of labeled M2 macrophages were administrated via subcutaneous injection into six regions on the dorsum of a nude mice, and NIR-II images were acquired subsequently in a time course. Figures 2(c1)–2(c6) demonstrated that the NIR-II imaging system was able to visualize as low as 5×10^2 labeled M2 macrophages.

Concentration of M2 macrophages in the tendon tissue during the first 7 days after injury was reported to be approximately $1 \times 10^4/mm^3$ [30]. Since the volume of the supraspinatus tendon of mice used in the current study averaged 10 mm^3 (5 mm × 2 mm × 1 mm), 2×10^5 cells were chosen for the subsequent cell therapy *in vivo* with the aim of doubling the concentration of M2 macrophages in the tendon tissue.

Despite reports of M2 macrophage on promotion of healing and regeneration, growing evidence questions the best timing of M2 macrophage administration or activation as a pro-healing and anti-inflammatory therapy [1, 8, 12]. Healing of the surgically repaired supraspinatus has been proven facing an obstacle that the original structure could not be regenerated completely and efficient solutions to improve the healing outcome are still under discover. To explore the improvement by M2 macrophage therapy to this process, surgical detachment and repair were performed according to previous studies to establish a murine model of acute injury and surgical repair of the supraspinatus tendon (Fig. S1 in the ESM) [21]. To investigate whether the timing of M2 macrophage therapy matters, the ICT and the DCT were compared, in which the PbS QDs labeled M2 macrophages were injected into the glenohumeral joint cavity and subacromial space either immediately after repair (the ICT group) or on the 7th day after repair (the DCT group) (Fig. 3(a)). Immunohistochemical analysis demonstrated that the number of native M2 macrophages within the surgically repaired supraspinatus tendon was highest on day 7 post-operation (Fig. S2 in the ESM). Accordingly, the delayed therapy was performed at the identical timepoints. Representative NIR-II images matched with X-ray images of the shoulder of mice after cell therapy were demonstrated in Fig. 3(b), with corresponding NIR-II intensity and the endurance of NIR-II signal in the region of tendon analyzed in Figs. 3(c)–3(f). Initially, the comparison of endurance of NIR-II signal of the two groups revealed remarkably longer retention of M2 macrophages in the region of the repaired supraspinatus tendon in the DCT group (32.7 ± 4.0 vs. 12.7 ± 2.3 days, p = 0.031) (Fig. 3(c)). Secondly, a rise of NIR-II intensity measured in the region of the supraspinatus tendon was detected from day 1 to 7 post-cell therapy in the DCT group, and a peak was observed on day 7 (Fig. 3(d)). After that, a steady decrease of NIR-II intensity occurred and lasted until the end of observation. Of note, the NIR-II intensity in the ICT group decreased over time, displaying a pattern different from the DCT group. As a result, the NIR-II signal intensity was similar between the two groups on day 1 and 3 post-injection, but the signal intensity of the DCT group remained profoundly higher in all the following measurements, which indicates that a larger number of M2 macrophages were detected around the repairing tendon in the DCT group at these timepoints (Fig. 3(d)). The signal intensity of the IT QDs and DT QDs groups decreased monotonically during the 28-day observation period, and there was no statistically significant difference in the fluorescence duration between the two groups (Fig. S3 in the ESM). Besides, the ratio of the NIR-II intensity measured in the region of the supraspinatus tendon to the shoulder increased throughout the observation in the DCT group, signaling continual cell accumulation towards the repaired tendon. Meanwhile, the ratio of the ICT group, which presented an increase from day 1 to 7 post-injection and a decrease afterwards, suggested that accumulation of the injected M2 macrophages towards the repaired tendon was reduced after the 7th day (Fig. 3(f)). These results suggested that the supraspinatus tendon in the inflammation period after surgical repair (days 0–7 post-operation) was less suitable for the accumulation and survival of M2 macrophages as compared to the repair period (days 5–14 post-operation) [31]. The finding is in the agreement with the

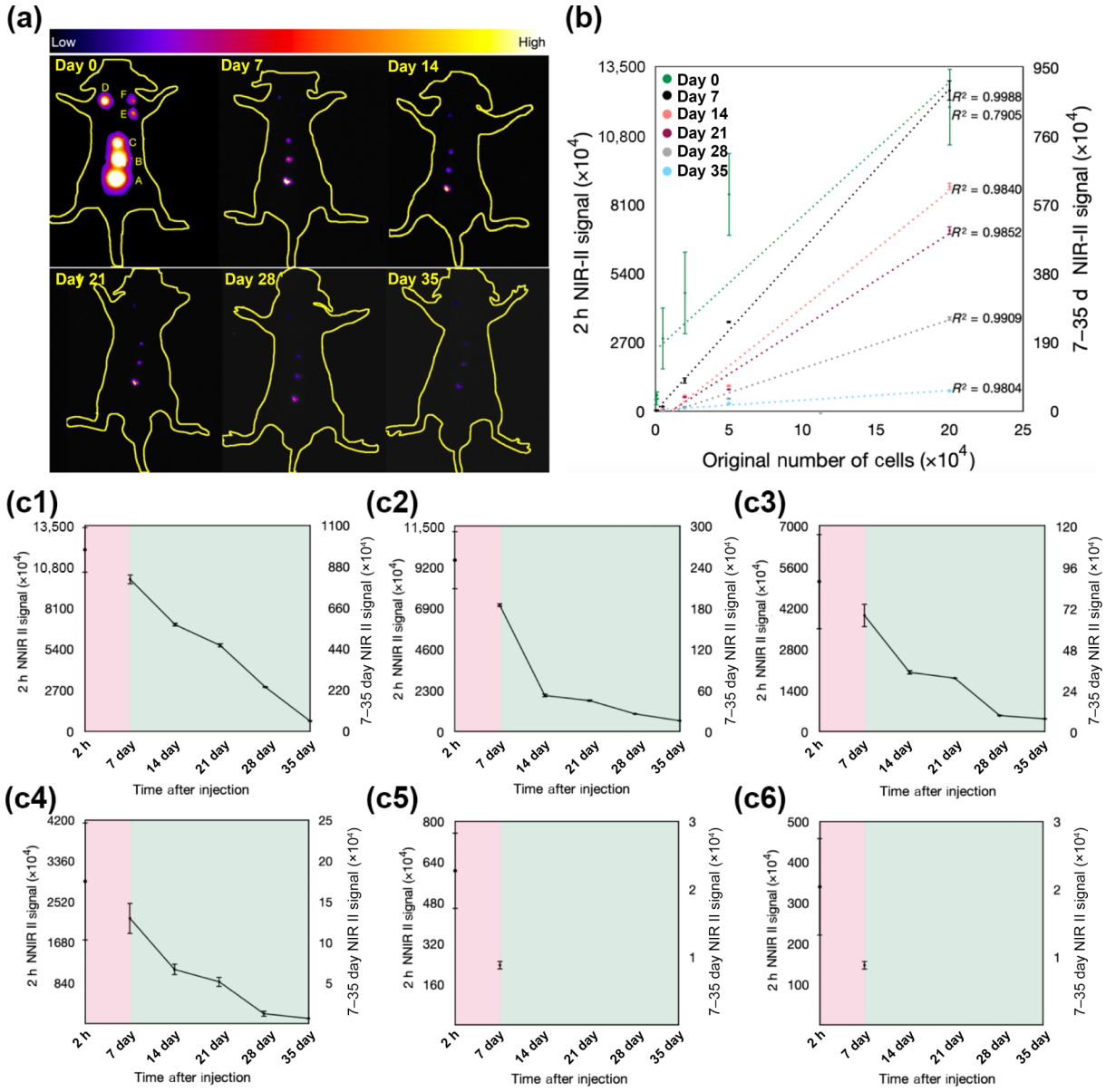

Figure 2 *In vivo* detection of sensitivity and stability of PbS QDs labeled M2 macrophages. (a) Representative *in vivo* NIR-II images (λ_{ex}: 808 nm, exposure time: 250 ms) of different numbers of subcutaneously injected PbS QDs labeled M2 macrophages (A-2 × 105, B-5 × 104, C-2 × 104, D-5 × 103, E-1 × 103, and 5 × 102 cells) in a time course (λ_{ex}: 808 nm, exposure time: 250 ms). (b) The linear relationship between the original number of injected M2 macrophages and NIR-II signal intensity in a time course measured from (a). Results of linear fitting are demonstrated by dotted curves. ((c1)–(c6)) NIR-II intensity of points A–F in a time course analyzed from (a) ($N = 3$). Data are represented as the mean ± SD.

previous observations that postponed introduction of reparative cells may contribute to survival of these cells, likely due to the facts that hypoxia within injured tissues becomes less severe and the newly formed granulation tissue provides more adherence sites [7].

The above findings suggested that the injected M2 macrophages gathered around the repairing structure, yet it is to be clarified whether the injected cells react to the chemical gradient within injured tissues and if the response is influenced by the time of administration. Thereby, migration of the injected M2 macrophages around the repaired tendon was analyzed as depicted (Fig. 4(a)). The position of the peak of NIR-II signal intensity measured in the region of the supraspinatus tendon was used to describe the position of the injected M2 macrophages within this region (Fig. 4(b)). Injected M2 macrophages were discovered to be moving towards the repairing structure in the ICT groups between day 1 and 7 post-injection, but retracted thereafter. In contrast, in the DCT group, the injected M2 macrophages approached the injury within the first 7 days and retained at the site throughout the observation period (Fig. 4(b)). Furthermore, the peak of the NIR-II signal intensity of the DCT group by the end of observation located nearer to the repairing structure than the one of ICT group.

To explore the mechanism behind the migration of M2 macrophages in the vicinity of the repairing supraspinatus tendon, mathematical analysis based on the Keller–Segel model [23] was performed using the NIR-II fluorescence images to present changes of the chemotaxis effect after cell therapy. Primarily, distributions of the chemical potential from the joint cavity to the lateral edge of the humeral head that attracts M2 macrophage were calculated as shown in Figs. 4(c) and 4(d). The mean chemical potential at each time point calculated from Figs. 4(c) and 4(d) showed increase in the mean chemical potential between day 1 and 7 post-injection in the ICT group with subsequent decline (Fig. 4(e)). In contrast, the mean chemical potential in the DCT group showed a steady increase over time (Fig. 4(e)). The chemotaxis effect of each group, which was determined by the value of positive slope of the chemical potential distribution, was demonstrated in Fig. 4(f). Compared with the DCT group that

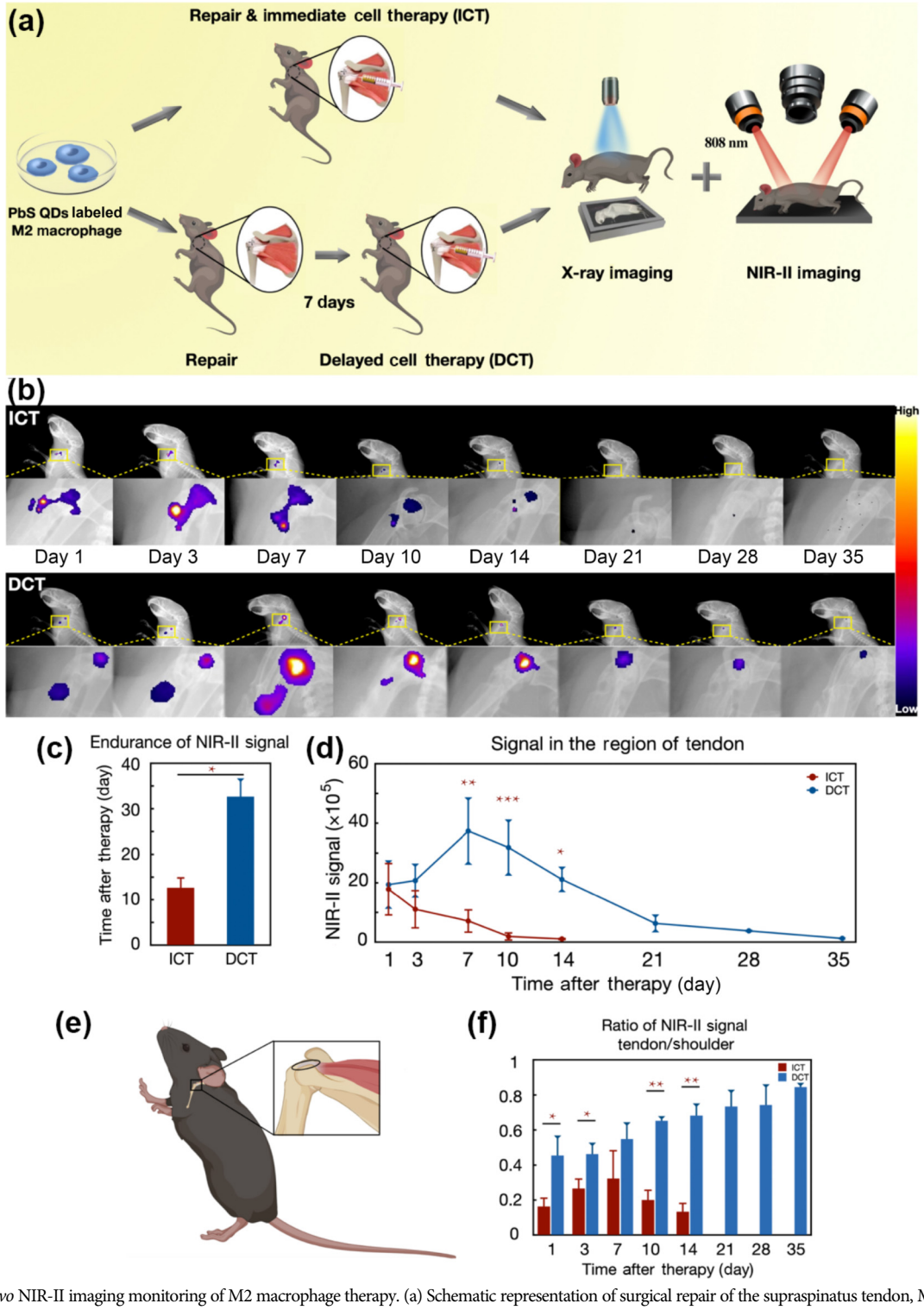

Figure 3 *In vivo* NIR-II imaging monitoring of M2 macrophage therapy. (a) Schematic representation of surgical repair of the supraspinatus tendon, M2 macrophage therapy, X-ray imaging, and NIR-II imaging strategies of the ICT and the DCT group. (b) Representative NIR-II images (λ_{ex}: 808 nm, exposure time: 250 ms) of the ICT and the DCT group demonstrating the distribution of injected M2 macrophages in a time course. (c) Endurance of NIR-II signal intensity in the region of supraspinatus tendon of the ICT and the DCT group. (d) The NIR-II signal intensity measured in the region of supraspinatus tendon of the ICT and the DCT group. (e) Schematic illustration of the region of analysis using NIR-II images (square: shoulder; ellipse: supraspinatus tendon). (f) Ratio of the NIR-II signal intensity measured in the region of supraspinatus tendon to the shoulder of the ICT and the DCT group (N = 3 to 4). Data are represented as the mean ± SD, with $^{*}p < 0.05$, $^{**}p < 0.01$, and $^{***}p < 0.001$ by student t test or Wilcoxon rank sum test.

generally displayed an increasing chemotaxis effect, the chemotaxis effect in the ICT group was considerably weaker and presented a progression from an incremental to a declining pattern. The two fitted curves (ICT, R^2 = 0.8156; DCT, R^2 = 0.8356) were significantly different, as indicated by the Kolmogorov–Smirnov test (P = 0.002).

To be noticed, the transformation of chemotaxis effect and cell migration of the ICT group, as shown in Figs. 4(e) and 4(f), matched the results of immunohistochemical analysis of native M2 macrophages (Fig. S2 in the ESM). Specifically, this analysis revealed that without cell therapy the number of native M2 macrophages within the tendon reached a peak on the 7th day after acute injury and surgical repair of the supraspinatus and began to decrease afterwards (Fig. S2 in the ESM). Nonetheless, the DCT group presented an apparently different curve, as shown in Fig. 4(f), which was attributed to the delayed cell therapy. In brief, the

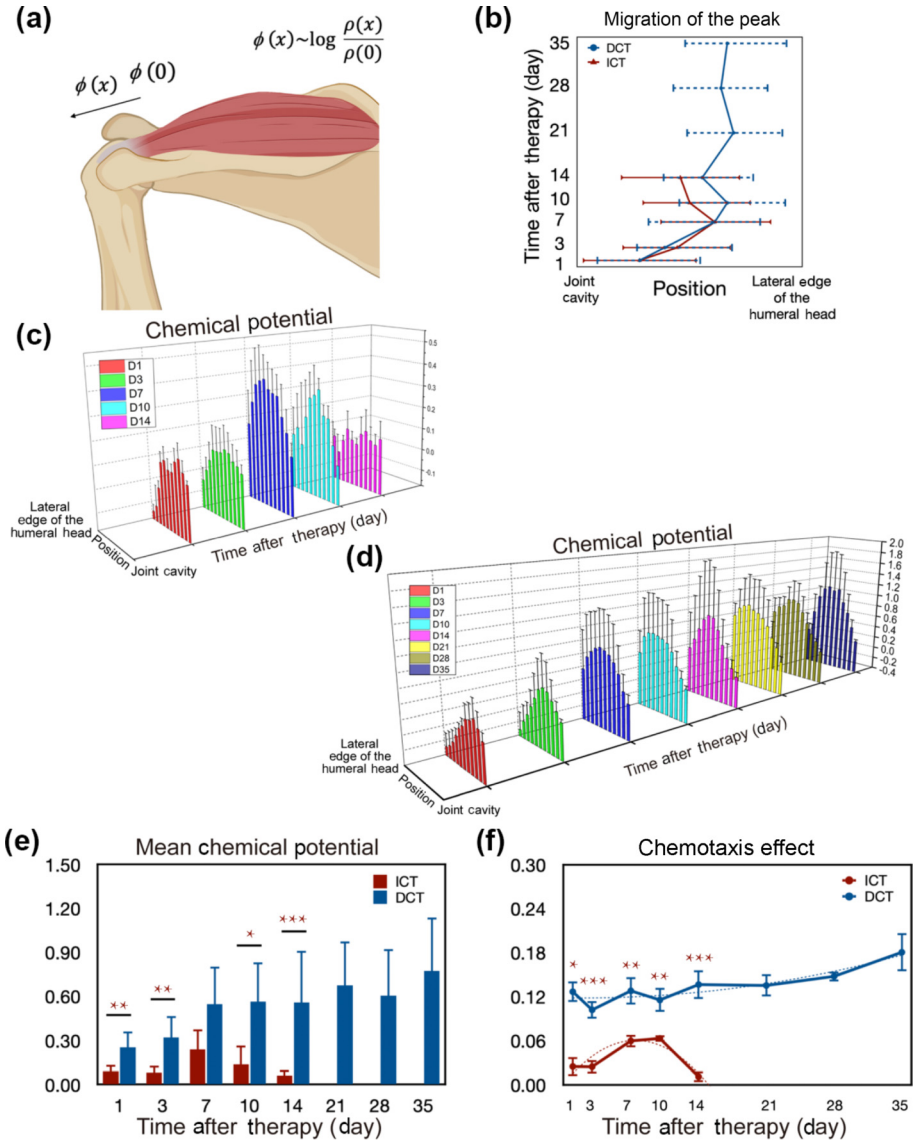

Figure 4 Analysis of M2 macrophage chemotaxis using NIR-II fluorescence images. (a) Schematic illustration of measuring the NIR-II signal along a line from the joint cavity to the lateral edge of the humeral head on NIR-II fluorescence images. ϕ(x) describes the chemical potential of point x, and $\rho(x)$ represents the number of cells detected at the point x. $\phi(0)$ and $\rho(0)$ represent the values of above parameters measured at the initial position of chemotaxis, respectively. (b) The position of the peak of NIR-II signal intensity measured along the line indicated by (a) of the ICT and the DCT group. Bars represent the region which is centered in the position of the peak and is covered 50% of area under curve (AUC). ((c) and (d)) The chemical potential from the joint cavity to the lateral edge of the humeral head of the ICT and the DCT groups, respectively. (e) The mean chemical potential in a time course calculated from ((c) and (d)). (f) The chemotaxis effect in a time course analyzed from ((c) and (d)). Results of polynomial fitting are demonstrated by dotted curves (N = 3 to 4). Data are represented as the mean ± SD, with $^{*}p < 0.05$, $^{**}p < 0.01$, and $^{***}p < 0.001$ by student t test or Wilcoxon rank sum test.

delayed therapy worked efficiently to change the chemotaxis effect, while the effect of the immediate therapy was restricted, implying that the timing of reparative cell therapy influenced its effect.

M2 macrophages yield diverse functions via immunomodulation. Therefore, analyses of peripheral leukocyte were conducted to inspect how the immune system responds to the immediate and the delayed M2 macrophage therapy (Fig. 5(a)). Results from day 15 to 30 post-operation were omitted in Fig. 5, as no significant differences were detected since day 10 (Fig. S4 in the ESM). As shown in Fig. 5(b1), the proportion of peripheral neutrophils of the ICT group was significantly lower than that of the controls on day 1. Apart from that, no difference was ever detected at other time points and in other leukocyte subsets between the ICT group and the controls (Figs. 5(b2)–5(b5)). Therefore, it could be deducted that the acute inflammatory response after tendon injury and surgical repair was probably decreased after immediate introduction of M2 macrophages, but overall, the response of immune system to the immediate therapy was inapparent. Conversely, the proportion of neutrophil and monocyte in the peripheral blood of mice treated by the DCT extensively surged on day 1 post-cell therapy as compared to the controls (Figs. 5(b1) and 5(b3)), while the lymphocyte/monocyte ratio (LMR) went down substantially (Fig. 5(b4)). These shifts resembling the acute inflammatory response (Fig. S5 in the ESM) might be attributed to the immune response triggered by injection as a trauma. Notably, an apparently increased count of total leukocytes in the DCT group as compared to the control group was observed on day 5 (Fig. 5(b5)), which was often linked to enhanced inflammatory response; meanwhile, the proportion of monocyte declined (Fig. 5(b3)), thus an increased LMR that was recognized as a sign of resolving inflammation was detected (Fig. 5(b4)) [32, 33]. These changes that were different from typical inflammatory response as presented by Fig. S5 in the ESM, which were presented only in the DCT group, could be interpreted as the immunomodulatory effect due to injected M2 macrophages. The results of peripheral blood tests unveiled potential for the M2 macrophages to function in the repair phase (days 5–14 post-operation) rather than the

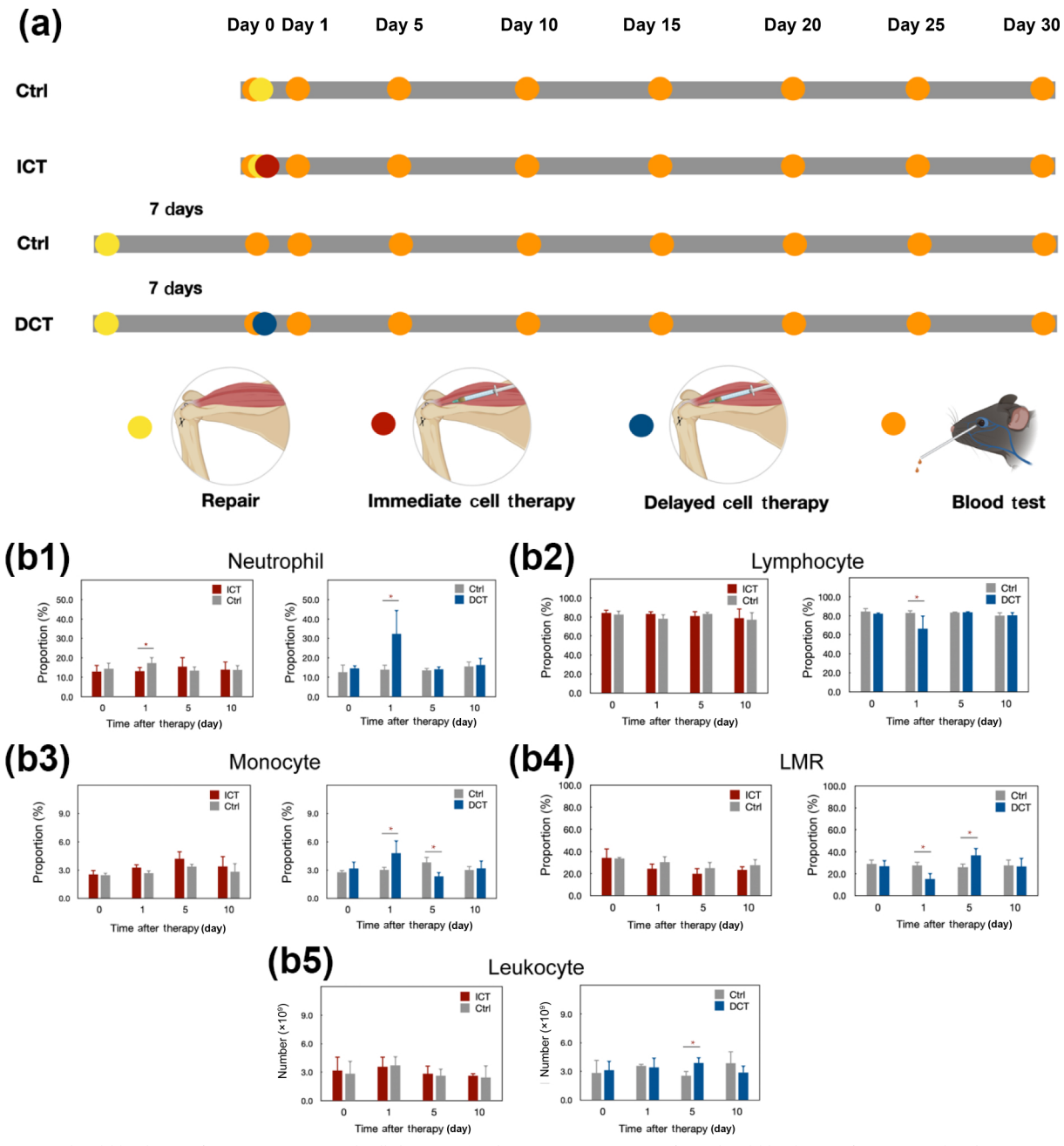

Figure 5 Peripheral blood tests after repair surgery and cell therapy. (a) Schematic representation of peripheral blood tests of mice treated with M2 macrophage therapy and mice served as controls. ((b1)–(b5)) Results of peripheral blood tests with statistically significant differences (N = 3 to 4). Data are presented as the mean ± SD, with *$p < 0.05$ by student t test or Wilcoxon rank sum test.

inflammation phase (days 0–7 post-operation) after acute injury and surgical repair of the supraspinatus tendon. This was in consistent with a forementioned findings obtained from NIR-II fluorescence images (Figs. 3(d)–3(f), 4(e), and 4(f)), demonstrating that the response to M2 macrophage therapy varies with the timing of application.

In clinical practice, non-invasive and longitudinal investigation of tendon integrity after rotator cuff repair is completed by mMRI, and the SNQ is calculated from MRI images, which negatively correlates with the water content of tissues. This approach is widely used to assess maturation of the repaired supraspinatus tendon [34, 35]. It was demonstrated that the SNQ of the supraspinatus tendon primarily increases in response to inflammation after repair surgery and thereafter changes to a continual decline as maturation of the repaired tendon progresses [36]. To follow the change of the repaired supraspinatus tendon after M2 macrophage therapy, micro-MRI scans were performed at 2, 5, and 9 weeks post-operation (Fig. 6(a)). An increase in the SNQ of the repaired tendon was found at 5 weeks post-operation followed by a decrease at 9 weeks post-operation in the ICT and the control groups (Figs. 6(b) and 6(c)), while the SNQ of repaired tendon appeared to be decreasing at both time points in the DCT group (Figs. 6(b) and 6(c)). Hence, at 5 weeks post-operation, significantly lower SNQ of repaired tendon was presented in the DCT group, demonstrating accelerated maturation of the repaired tendon by the delayed M2 macrophage therapy. Consequently, it was concluded that maturation of the repaired tendon was accelerated only by the delayed M2 macrophage therapy, maintaining the importance of administrating reparative cells with a proper timing.

At 9 weeks post-operation, the mice in each group were sacrificed. The tendon-bone insertion connectivity and morphology were studied through histopathological analysis using H&E staining, Masson staining, Sirius red staining, and safranin-O staining (Fig. 7(a)). Tendon of the DCT group mainly consists of type I collagen (red fibers with Sirius red staining under

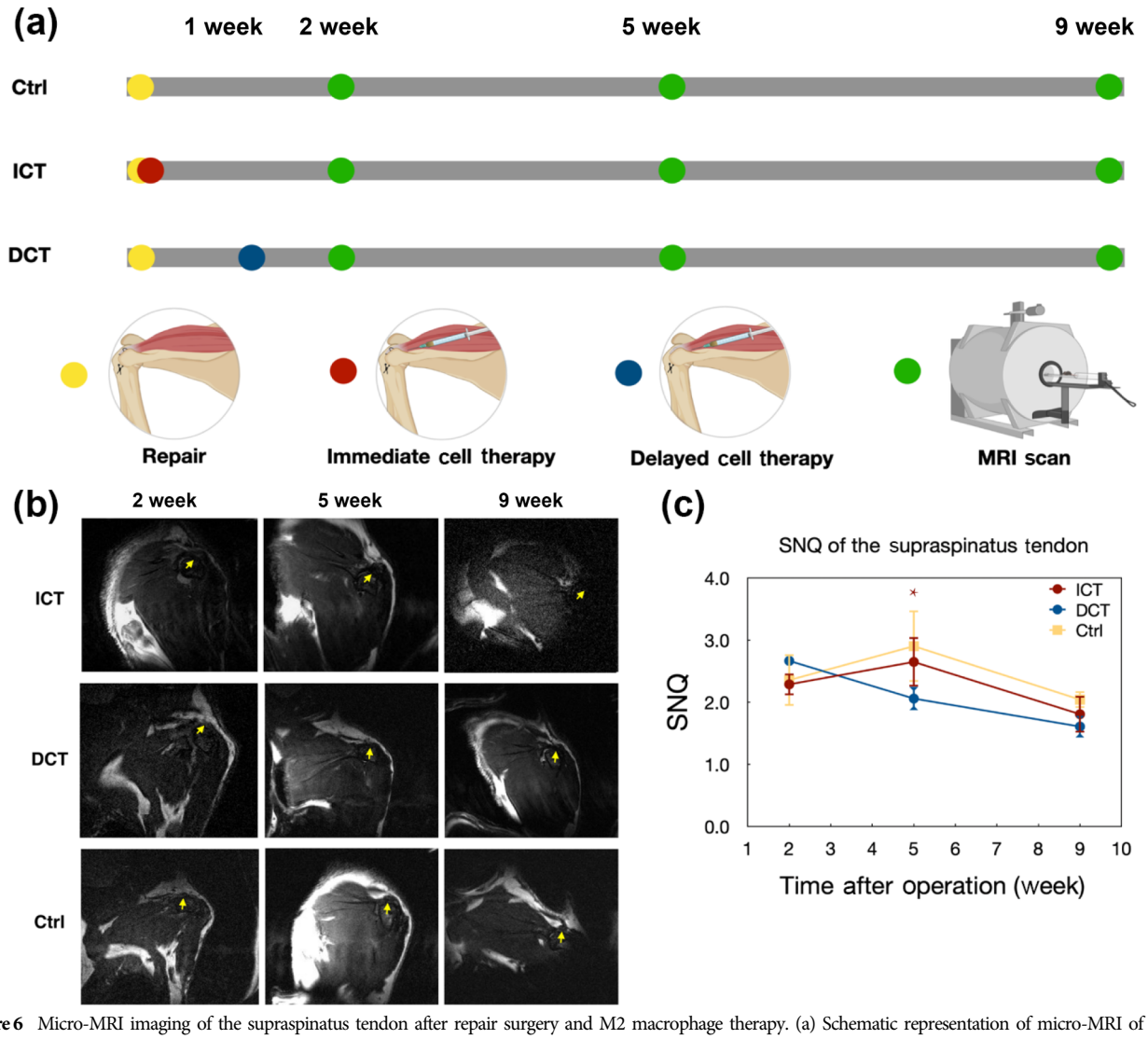

Figure 6 Micro-MRI imaging of the supraspinatus tendon after repair surgery and M2 macrophage therapy. (a) Schematic representation of micro-MRI of mice treated with M2 macrophage therapy and mice as controls. (b) Representative oblique coronal MRI images of the operated shoulder of the ICT, the DCT and the control group in a time course. Arrows indicate the supraspinatus tendon near the insertion. (c) SNQ of the supraspinatus tendon analyzed from MRI images ($N = 3$ to 4). Data are presented as the mean ± SD, with $^*p < 0.05$ as compared with the control group by one-way analysis of variance (ANOVA).

polarizing light), while tendon of the ICT and the control group contains type III collagen (green fibers with Sirius red staining under polarizing light). To complete a semi-quantitative evaluation of healing, histological examination scores based on previously reported systems for supraspinatus tendon and tendon–bone insertion were calculated (Fig. 7(b) and Fig. S6 in the ESM) [20, 25, 26]. It revealed that the DCT group showed better tendon quality with better total score and fiber arrangement than the other two groups (Fig. 7(b) and Fig. S6 in the ESM). The difference in the total score between the ICT and the control group was not statistically significant, indicating that immediate M2 macrophage administration neither impairs nor improves the healing outcome, which was probably due to restricted accumulation and a relatively short stay of injected M2 macrophages within the repaired structure (Figs. 3(d)–3(f)). Results of histological assessments confirmed that the outcome of M2 macrophage therapy was linked to the timing of administration.

4 Conclusions

In general, M2 macrophage therapy applied on the 7th day after repair improved the healing outcome after acute injury and surgical repair of the supraspinatus tendon rather than an immediate M2 macrophage therapy by comprehensively judging from the results of peripheral blood tests, MRI imaging, and histological analysis, suggesting that the pro-healing nature of M2 macrophages may be facilitated by their delayed administration to the injury site. By other words, the best timing of M2 macrophage therapy was not missed with a delay, conversely, the therapy made a relatively better performance with such a delay. Moreover, the current study, by employing NIR-II imaging, realized *in vivo* monitoring of the injected M2 macrophages, thus highlighting a possible explanation of the advantage of the delayed therapy, which promotes accumulation and prolongs retention of administrated cells within the healing structure, that was associated with the synchronization between the state of micro-environment and the pro-healing property of M2 macrophages. The findings of the current study call for reconsideration of the timing of pro-healing therapies, especially when being used after an acute injury or surgical procedure, in which the evidence acquired by *in vivo* tracking of cells should be emphasized.

Acknowledgements

This animal research received the approval of ethics by Ethics Committee of Fudan University (No. 202208005Z). This work was supported by the National Natural Science Foundation of China (Nos. 81972129, 82072521, and 82111530200), Shanghai Talent

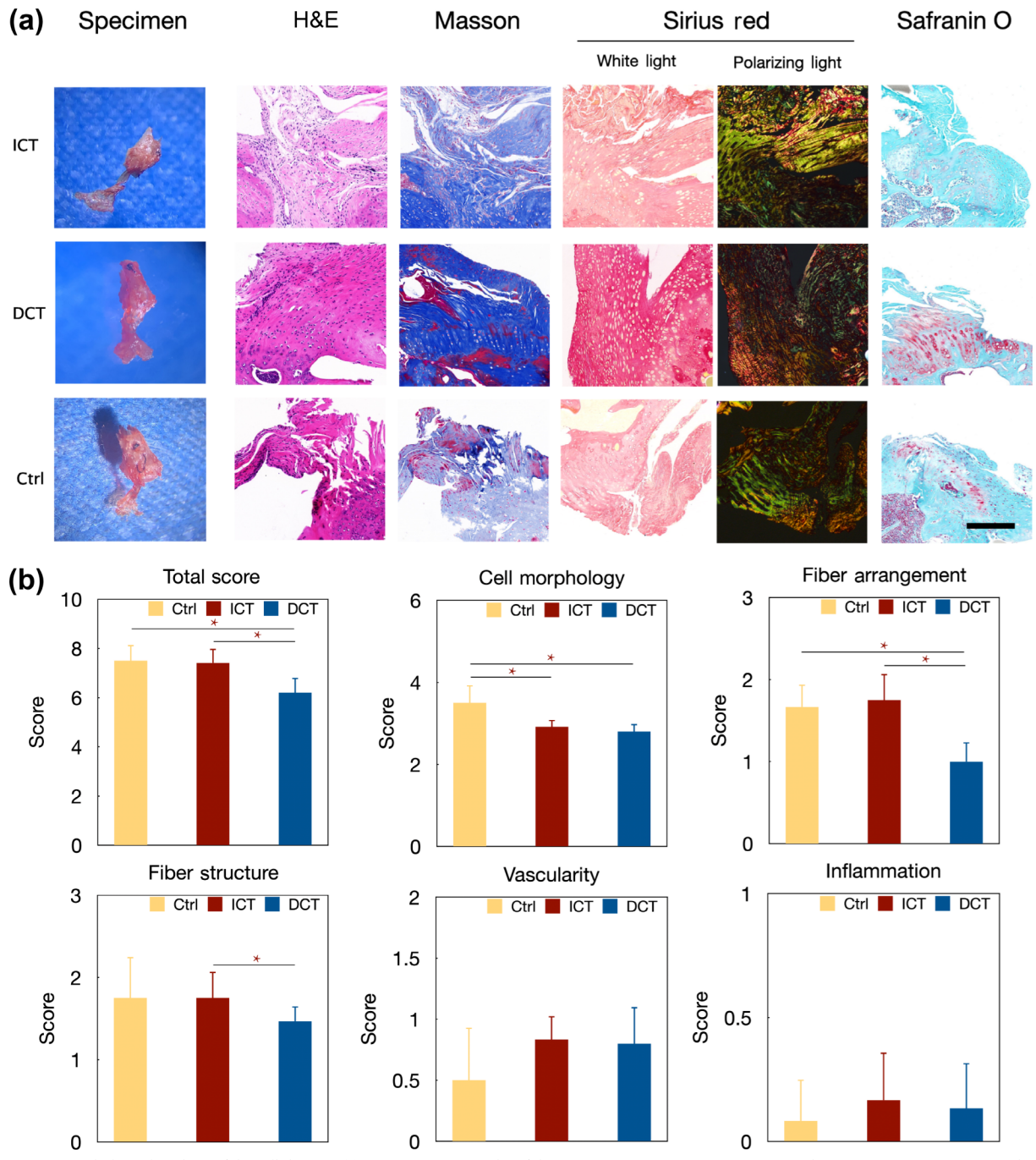

Figure 7 Histopathological analysis of the cell therapy. (a) Representative graphs of the specimens, H & E staining micrographs, Masson staining micrographs, Sirius red staining micrographs (white light and polarizing light view), and safranin O staining micrographs of the insertion of supraspinatus tendon from the ICT, the DCT, and the control group. Scale bar: 200 μm. (b) Histological examination scores of the supraspinatus tendon near the tendon-bone insertion of each group (N = 3 to 4). Data are presented as the mean ± SD, with $^*p < 0.05$ by one-way ANOVA.

Development Funding Scheme (No. 2020080), and Shanghai Committee of Science and Technology (Nos. 22DZ2204900 and 23ZR1445700). J. Chen and N. T. K. Thanh thank the Royal Society and National Natural Science Foundation of China for the International Exchanges program for funding. The authors thank Hao Chen and his team from Shanghai Institute of Materia Medica, Chinese Academy of Sciences for providing the NIR-II fluorescence imaging instrument.

Electronic Supplementary Material: Supplementary material (mouse model construction, immunohistochemistry analysis, results of *in vivo* NIR-II imaging, results of peripheral blood tests, and histological examination scores) is available in the online version of this article at https://doi.org/10.1007/s12274-023-6363-x.

References

[1] Dreymueller, D.; Denecke, B.; Ludwig, A.; Jahnen-Dechent, W. Embryonic stem cell-derived M2-like macrophages delay cutaneous wound healing. *Wound Repair Regen.* **2013**, *21*, 44–54.

[2] Duan, J.; Liu, X. S.; Wang, H. L.; Guo, S. W. The M2a macrophage subset may be critically involved in the fibrogenesis of endometriosis in mice. *Reprod. Biomed. Online* **2018**, *37*, 254–268.

[3] Gulotta, L. V.; Kovacevic, D.; Ehteshami, J. R.; Dagher, E.; Packer, J. D.; Rodeo, S. A. Application of bone marrow-derived mesenchymal stem cells in a rotator cuff repair model. *Am. J. Sports. Med.* **2009**, *37*, 2126–2133.

[4] Murray, P. J.; Allen, J. E.; Biswas, S. K.; Fisher, E. A.; Gilroy, D. W.; Goerdt, S.; Gordon, S.; Hamilton, J. A.; Ivashkiv, L. B.; Lawrence, T. et al. Macrophage activation and polarization: Nomenclature and experimental guidelines. *Immunity* **2014**, *41*, 14–20.

[5] Arnold, L.; Henry, A.; Poron, F.; Baba-Amer, Y.; van Rooijen, N.; Plonquet, A.; Gherardi, R. K.; Chazaud, B. Inflammatory monocytes recruited after skeletal muscle injury switch into antiinflammatory macrophages to support myogenesis. *J. Exp. Med.* **2007**, *204*, 1057–1069.
[6] Lucas, T.; Waisman, A.; Ranjan, R.; Roes, J.; Krieg, T.; Müller, W.; Roers, A.; Eming, S. A. Differential roles of macrophages in diverse phases of skin repair. *J. Immunol.* **2010**, *184*, 3964–3977.
[7] Contreras-Muñoz, P.; Torrella, J. R.; Venegas, V.; Serres, X.; Vidal, L.; Vila, I.; Lahtinen, I.; Viscor, G.; Martínez-Ibáñez, V.; Peiró, J. L. et al. Muscle precursor cells enhance functional muscle recovery and show synergistic effects with postinjury treadmill exercise in a muscle injury model in rats. *Am. J. Sports Med.* **2021**, *49*, 1073–1085.
[8] Chamberlain, C. S.; Clements, A. E. B.; Kink, J. A.; Choi, U.; Baer, G. S.; Halanski, M. A.; Hematti, P.; Vanderby, R. Extracellular vesicle-educated macrophages promote early achilles tendon healing. *Stem Cells.* **2019**, *37*, 652–662.
[9] Jayme, T. S.; Leung, G.; Wang, A.; Workentine, M. L.; Rajeev, S.; Shute, A.; Callejas, B. E.; Mancini, N.; Beck, P. L.; Panaccione, R. et al. Human interleukin-4-treated regulatory macrophages promote epithelial wound healing and reduce colitis in a mouse model. *Sci. Adv.* **2020**, *6*, eaba4376.
[10] Jetten, N.; Roumans, N.; Gijbels, M. J.; Romano, A.; Post, M. J.; de Winther, M. P. J.; van der Hulst, R. R. W. J.; Xanthoulea, S. Wound administration of M2-polarized macrophages does not improve murine cutaneous healing responses. *PLoS One.* **2014**, *9*, e102994.
[11] D'Alessio, F. R.; Craig, J. M.; Singer, B. D.; Files, D. C.; Mock, J. R.; Garibaldi, B. T.; Fallica, J.; Tripathi, A.; Mandke, P.; Gans, J. H. et al. Enhanced resolution of experimental ARDS through IL-4-mediated lung macrophage reprogramming. *Am. J. Physiol. Lung Cell. Mol. Physiol.* **2016**, *310*, L733–L746.
[12] Francos-Quijorna, I.; Amo-Aparicio, J.; Martinez-Muriana, A.; López-Vales, R. IL-4 drives microglia and macrophages toward a phenotype conducive for tissue repair and functional recovery after spinal cord injury. *Glia.* **2016**, *64*, 2079–2092.
[13] Hunter, M. M.; Wang, A.; Parhar, K. S.; Johnston, M. J. G.; Van Rooijen, N.; Beck, P. L.; McKay, D. M. *In vitro*-derived alternatively activated macrophages reduce colonic inflammation in mice. *Gastroenterology* **2010**, *138*, 1395–1405.
[14] Jetten, N.; Donners, M. M. P. C.; Wagenaar, A.; Cleutjens, J. P. M.; van Rooijen, N.; de Winther, M. P. J.; Post, M. J. Local delivery of polarized macrophages improves reperfusion recovery in a mouse hind limb ischemia model. *PLoS One* **2013**, *8*, e68811.
[15] Raimondo, T. M.; Mooney, D. J. Functional muscle recovery with nanoparticle-directed M2 macrophage polarization in mice. *Proc. Natl. Acad. Sci. USA* **2018**, *115*, 10648–10653.
[16] Chen, G. Y.; Roy, I.; Yang, C. H.; Prasad, P. N. Nanochemistry and nanomedicine for nanoparticle-based diagnostics and therapy. *Chem. Rev.* **2016**, *116*, 2826–2885.
[17] Li, C. Y.; Zhang, Y. J.; Wang, M.; Zhang, Y.; Chen, G. C.; Li, L.; Wu, D. M.; Wang, Q. B. *In vivo* real-time visualization of tissue blood flow and angiogenesis using Ag_2S quantum dots in the NIR-II window. *Biomaterials* **2014**, *35*, 393–400.
[18] Wan, H.; Yue, J. Y.; Zhu, S. J.; Uno, T.; Zhang, X. D.; Yang, Q. L.; Yu, K.; Hong, G. S.; Wang, J. Y.; Li, L. L. et al. A bright organic NIR-II nanofluorophore for three-dimensional imaging into biological tissues. *Nat. Commun.* **2018**, *9*, 1171.
[19] Welsher, K.; Sherlock, S. P.; Dai, H. J. Deep-tissue anatomical imaging of mice using carbon nanotube fluorophores in the second near-infrared window. *Proc. Natl. Acad. Sci. USA* **2011**, *108*, 8943–8948.
[20] Yang, Y. M.; Chen, J.; Shang, X. L.; Feng, Z. J.; Chen, C.; Lu, J. Y.; Cai, J. Y.; Chen, Y. Z.; Zhang, J.; Hao, Y. F. et al. Visualizing the fate of intra-articular injected mesenchymal stem cells *in vivo* in the second near-infrared window for the effective treatment of supraspinatus tendon tears. *Adv. Sci.* **2019**, *6*, 1901018.
[21] Lebaschi, A. H.; Deng, X. H.; Camp, C. L.; Zong, J. C.; Cong, G. T.; Carballo, C. B.; Album, Z.; Rodeo, S. A. Biomechanical, histologic, and molecular evaluation of tendon healing in a new murine model of rotator cuff repair. *Arthros.: J. Arthros. Relat. Surg.* **2018**, *34*, 1173–1183.
[22] Chen, M.; Chen, Y. Z.; Feng, S. J.; Dong, S. X.; Sun, L. Y.; Li, H. Z.; Chen, F. C.; Thanh, N. T. K.; Li, Y. X.; Chen, S. Y. et al. SWIR fluorescence imaging *in vivo* monitoring and evaluating implanted M2 macrophages in skeletal muscle regeneration. *Engineering*, in press. DOI: 10.1016/j.eng.2023.05.010.
[23] Keller, E. F.; Segel, L. A. Model for chemotaxis. *J. Theor. Biol.* **1971**, *30*, 225–234.
[24] Zhong, Y. T.; Jin, W. H.; Gao, H.; Sun, L. Y.; Wang, P.; Zhang, J.; Ong, M. T. Y.; Sai Chuen Bruma, F.; Chen, S.; Chen, J. A knitted PET patch enhances the maturation of regenerated tendons in bridging reconstruction of massive rotator cuff tears in a rabbit model. *Am. J. Sports Med.* **2023**, *51*, 901–911.
[25] Chen, J. M.; Yu, Q.; Wu, B.; Lin, Z.; Pavlos, N. J.; Xu, J. K.; Ouyang, H. W.; Wang, A.; Zheng, M. H. Autologous tenocyte therapy for experimental Achilles tendinopathy in a rabbit model. *Tissue Eng. Part A.* **2011**, *17*, 2037–2048.
[26] Cong, S.; Sun, Y. Y.; Lin, J. R.; Liu, S. H.; Chen, J. W. A Synthetic graft with multilayered co-electrospinning nanoscaffolds for bridging massive rotator cuff tear in a rat model. *Am. J. Sports Med.* **2020**, *48*, 1826–1836.
[27] Kong, Y. F.; Chen, J.; Fang, H. W.; Heath, G.; Wo, Y.; Wang, W. L.; Li, Y. X.; Guo, Y.; Evans, S. D.; Chen, S. Y. et al. Highly fluorescent ribonuclease-a-encapsulated lead sulfide quantum dots for ultrasensitive fluorescence *in vivo* imaging in the second near-infrared window. *Chem. Mater.* **2016**, *28*, 3041–3050.
[28] Dong, S. X.; Feng, S. J.; Chen, Y. Z.; Chen, M.; Yang, Y. M.; Zhang, J.; Li, H. Z.; Li, X. T.; Ji, L.; Yang, X. et al. Nerve suture combined with ADSCs injection under real-time and dynamic NIR-II fluorescence imaging in peripheral nerve regeneration *in vivo*. *Front. Chem.* **2021**, *9*, 676928.
[29] Ying, W.; Cheruku, P. S.; Bazer, F. W.; Safe, S. H.; Zhou, B. Y. Investigation of macrophage polarization using bone marrow derived macrophages. *J. Vis. Exp.* **2013**, *23*, 50323.
[30] Marsolais, D.; Côté, C. H.; Frenette, J. Neutrophils and macrophages accumulate sequentially following Achilles tendon injury. *J. Orthop. Res.* **2001**, *19*, 1203–1209.
[31] Angeline, M. E.; Rodeo, S. A. Biologics in the management of rotator cuff surgery. *Clin. Sports Med.* **2012**, *31*, 645–663.
[32] Mandaliya, H.; Jones, M.; Oldmeadow, C.; Nordman, I. I. C. Prognostic biomarkers in stage IV non-small cell lung cancer (NSCLC): Neutrophil to lymphocyte ratio (NLR), lymphocyte to monocyte ratio (LMR), platelet to lymphocyte ratio (PLR) and advanced lung cancer inflammation index (ALI). *Transl. Lung. Cancer Res.* **2019**, *8*, 886–894.
[33] Sun, Y. Y.; Lin, J. R.; Luo, Z. W.; Chen, J. W. Preoperative lymphocyte to monocyte ratio can Be a prognostic factor in arthroscopic repair of small to large rotator cuff tears. *Am. J. Sports Med.* **2020**, *48*, 3042–3050.
[34] Ahn, J. H.; Lee, S. H.; Choi, S. H.; Lim, T. K. Magnetic resonance imaging evaluation of anterior cruciate ligament reconstruction using quadrupled hamstring tendon autografts: Comparison of remnant bundle preservation and standard technique. *Am. J. Sports Med.* **2010**, *38*, 1768–1777.
[35] Li, H.; Tao, H. Y.; Cho, S.; Chen, S.; Yao, Z. J.; Chen, S. Y. Difference in graft maturity of the reconstructed anterior cruciate ligament 2 years postoperatively: A comparison between autografts and allografts in young men using clinical and 3.0-T magnetic resonance imaging evaluation. *Am. J. Sports Med.* **2012**, *40*, 1519–1526.
[36] Liu, S. H.; Xie, Y. X.; Chen, Q. Y.; Sun, Y. Y.; Ding, Z. C.; Zhang, Y. H.; Chen, S. Y.; Chen, J. W. Tendon healing progression evaluated with magnetic resonance imaging signal intensity and its correlation with clinical outcomes within 1 year after rotator cuff repair with the suture-bridge technique. *Am. J. Sports Med.* **2020**, *48*, 697–705.